ACS Energy LETTERS

http://pubs.acs.org/journal/aelccp

Differentiating between Ion Transport and Plating–Stripping Phenomena in Magnesium Battery Electrolytes Using *Operando* Raman Spectroscopy

Rudra N. Samajdar,[‡] Sofia Marchesini,[‡] Scott A. Brown, Stuart D. Robertson, Keith R. Paton, Andrew J. Pollard, and Andrew J. Wain*

Cite This: https://doi.org/10.1021/acsenergylett.3c00279

Read Online

ACCESS | Metrics & More | Article Recommendations | Supporting Information

ABSTRACT: Understanding metal plating–stripping and mass transport processes is necessary for the development of new electrolytes for post-lithium energy storage applications. *Operando* vibrational spectroscopy is a valuable analytical tool for this purpose, enabling structural and chemical changes at electrode–electrolyte interfaces to be probed dynamically, under battery cycling conditions. In this work we apply *operando* Raman spectroscopy to characterize the behavior of the Mg based "all phenyl complex" $[Mg_2Cl_3]^+[AlPh_4]^-$ in tetrahydrofuran (THF), an exemplar electrolyte for emerging Mg battery technologies. We demonstrate that the observed electrolyte Raman band intensities vary reversibly with electrochemical cycling due to anion migration in response to the applied electric field, while Mg plating and stripping can be monitored independently through the broad background scattering intensity. Spectral measurements across different sites of the platinum working electrode indicate that the ion transport response is spatially heterogeneous, while the plating and stripping response is ubiquitous.

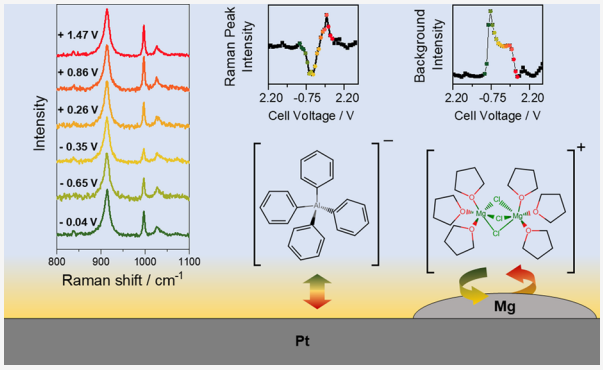

The high energy demands of modern life, balanced with worldwide efforts toward a carbon-neutral economy, require extensive improvements to existing energy storage technologies.[1,2] Developing post-Li energy storage is crucial due to geopolitical factors associated with material supply chains as well as fundamental limitations of electrodes in Li-based batteries.[3,4] In this domain, Mg-based technologies have emerged primarily due to advantages in Earth abundance and volumetric energy density.[5,6] Among the main factors still limiting the commercial realization of this technology is the lack of suitable electrolytes,[7] which require high ionic conductivity while allowing reversible electrochemical Mg plating and stripping.[8,9]

Analytical science has a critical role to play in the development of new electrolytes, by supporting improved understanding of interfacial processes and elucidation of degradation and failure mechanisms.[10,11] In this regard, *operando* spectroscopy, particularly vibrational methods such as Fourier transform infrared (FTIR) and Raman spectroscopy, are very useful because they allow direct observation of chemical speciation in electrolytes during electrochemical cycling.[12] Our groups have been active in this area and recently used attenuated total reflectance (ATR)-FTIR to re-examine one of the most widely used Mg electrolytes, the "all phenyl complex" (APC), which is a solution of dimagnesium trichloride tetraphenyl aluminate in tetrahydrofuran (THF) (active species $[Mg_2Cl_3]^+[AlPh_4]^-$, Figure 1a).[13−15] We demonstrated that the ATR-FTIR spectroelectrochemical response is very sensitive to interfacial transport effects and reveals crucial changes in coordination environment of the electroactive dinuclear cation and solvent during plating and stripping. Despite the potential insights available from FTIR, spectra can be difficult to interpret in isolation due to the dominance and convolution of multiple solvent bands in

Received: February 6, 2023
Accepted: March 15, 2023

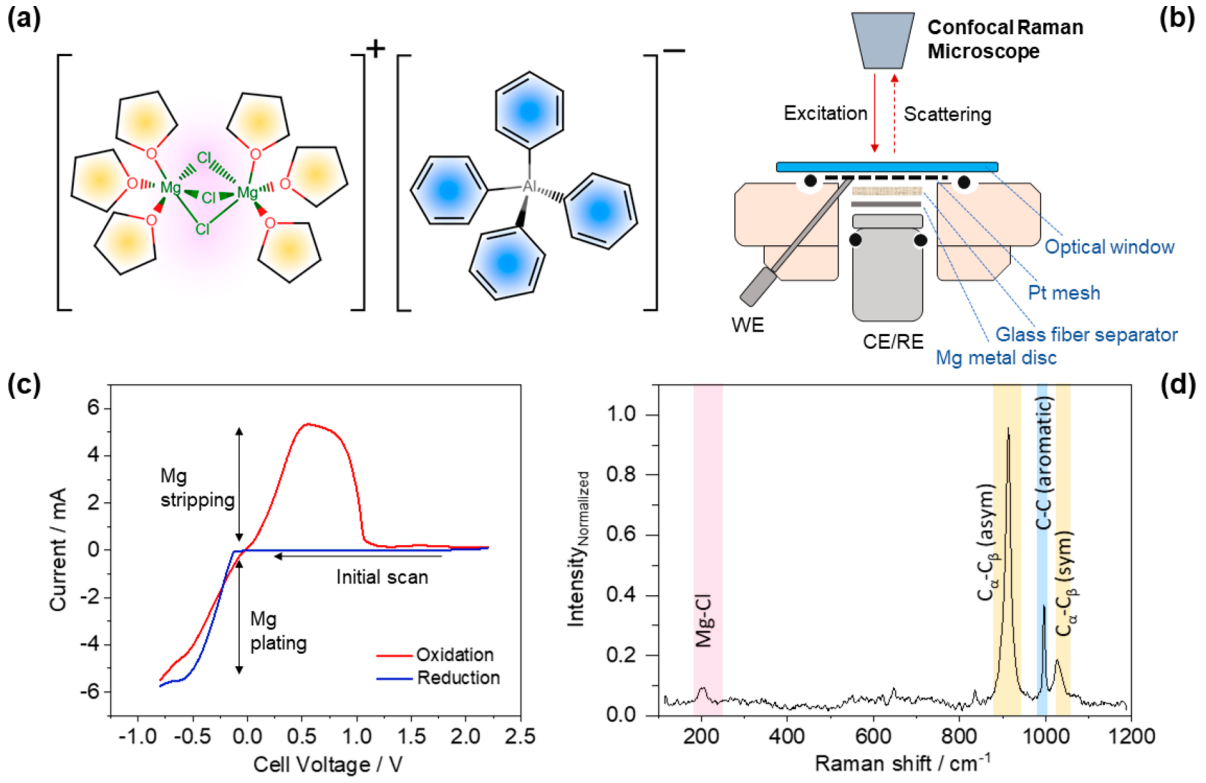

Figure 1. (a) Chemical structure of the ion pair present in APC electrolyte. (b) Schematic diagram of the spectroelectrochemical cell used for the *operando* Raman measurements. (c) Typical cyclic voltammogram of the APC electrolyte using the spectroelectrochemical cell, with the plating and stripping regions marked (see Supporting Information, section on Spectroelectrochemical Cell). (d) Typical Raman spectrum of APC electrolyte in the spectroelectrochemical cell recorded at OCV. Key bands in the spectrum are marked with colored rectangles; the corresponding chemical moieties responsible for these bands are illustrated with the same colors in panel a.

different local clustering and coordination states.[16] Raman spectroscopy offers a potential solution to this challenge, since the bulk solvent modes resulting from changes in dipole moment are typically inherently weaker in Raman scattering compared to FTIR. Similarly, vibrational modes that are FTIR silent are often active Raman scatterers. Hence, Raman spectroscopy is a complementary technique to FTIR, which may enable a cleaner separation of interfacial and bulk phenomena.[17,18]

Early development of organometallic Mg electrolytes primarily involved Raman spectroscopy for identifying the electroactive species in solutions—including different systems such as APC, related organohaloaluminum complexes in ethereal solvents, and $MgTFSI_2/MgCl_2$ [TFSI: Bis-(trifluoromethanesulfonyl)imide] solutions in dimethoxyethane.[19−21] With the introduction of inorganic complexes such as the magnesium aluminum chloride complex (a combination of $AlCl_3$ and $MgCl_2$ in organic solvent) and crystallographic identification of the electroactive dinuclear Mg cation, Raman spectroscopy was extended to understanding formation and conditioning processes.[21,22] However, most of the Raman reports on Mg battery electrolytes have been confined to *ex situ* studies which, given the inherent dynamic behavior of operating electrochemical systems, provide limited insights. To bridge this gap, here we report *operando* Raman spectroscopy of the APC electrolyte. We demonstrate that spectral background analysis and Raman peak fitting together allow investigation of both electrolyte ion migration in response to the applied electric field and Mg plating−stripping dynamics at the working electrode surface. In addition, we observe spatial heterogeneity demonstrating that these two phenomena can be probed independently.

In this study, we used a two-electrode spectroelectrochemical cell comprising a woven Pt gauze working electrode and Mg disc reference/counter electrode, which was filled with the APC electrolyte (Figure 1b). This cell allows optical access to the Pt gauze working electrode from the top via a sapphire optical window. The cell is geometrically equivalent to the coin cell-like configuration that we adopted for our recent ATR-FTIR study, thus facilitating direct comparison between *operando* techniques, while also allowing specific spatial variations to be resolved.

The cell was cycled through multiple potentiodynamic plating−stripping cycles, and an example cyclic voltammogram is depicted in Figure 1c which demonstrates reversible electrochemical plating and stripping of Mg (Table S1). Generally, we observed increasing plating and stripping currents with cycling, which we attribute to an increase in the number of Mg nucleation sites on the Pt gauze surface with repeated plating and stripping (see Figure S1).

We performed Raman spectroscopy using an 830 nm excitation laser (see Supporting Information, section on Raman Spectroscopy; Figure S2), which results in minimal fluorescence compared to excitation in the visible range (532 and 633 nm). Spectra were first collected across different regions of the Pt gauze electrode to check for spatial variations in the APC electrolyte bands. We recorded spectra in the uppermost regions of the Pt gauze that were in contact with the optical window, as well as regions on the lower part of the weave that were further from the window (Figure S3). The

https://doi.org/10.1021/acsenergylett.3c00279
ACS Energy Lett. XXXX, XXX, XXX−XXX

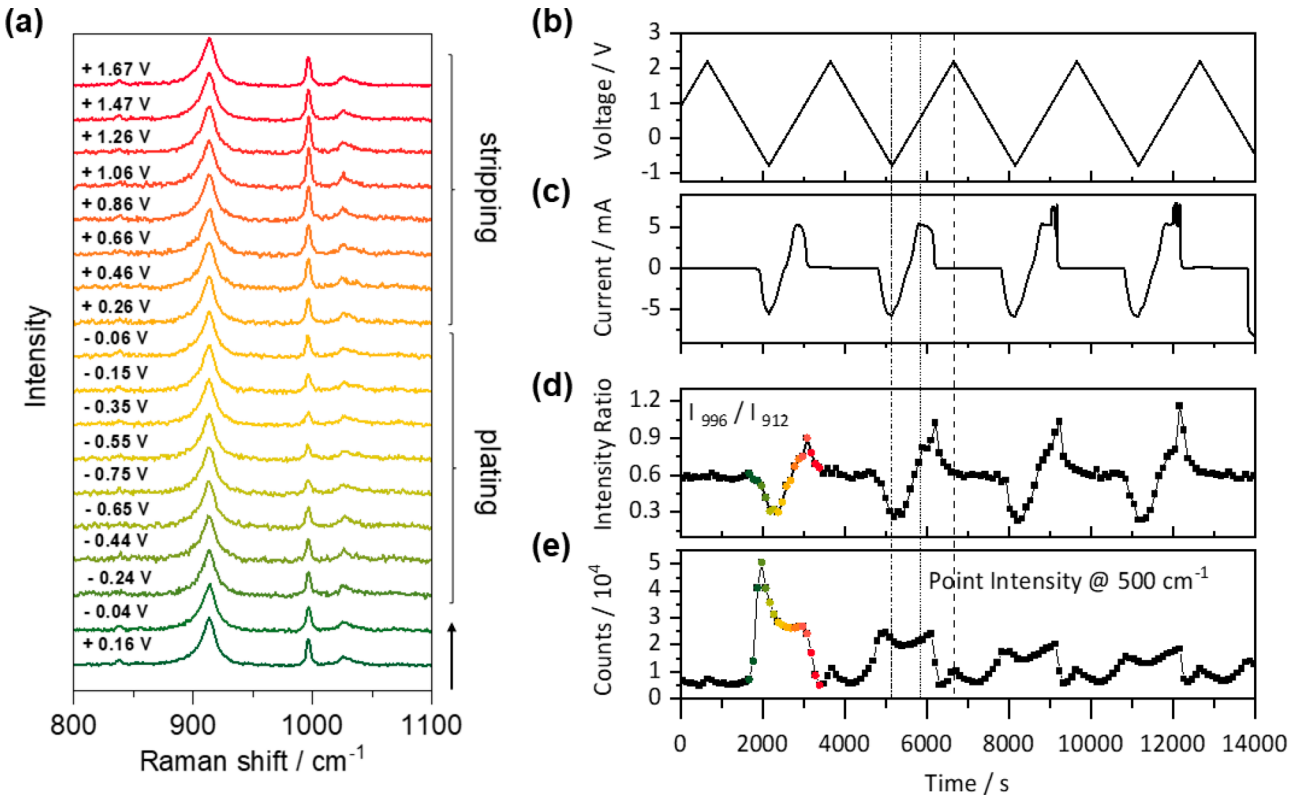

Figure 2. (a) *Operando* Raman spectra at different cell voltages. (b) Voltage and (c) current variations with cycling time during *operando* experiment. Raman spectroscopy metrics derived from spectra obtained during *operando* experiments showing (d) the intensity ratio of the 996 cm^{-1}/912 cm^{-1} peak and (e) point intensity at 500 cm^{-1}, reflecting background intensity variations. For parts d and e, the points on the first plating−stripping cycle are color-coded according to the corresponding spectra presented in part (a). Vertical lines are included in the second cycle to indicate the position of maximum voltage (dashed line), maximum current (dotted line) and minimum voltage and current (dash-dot line).

uppermost surface of the Pt gauze was found to exhibit weak Raman scattering due to the limited amount of electrolyte in the region sandwiched between the gauze and the window and also exhibits a scattering band associated with the sapphire window itself. Conversely, on the lower part of the weave, intense and more reproducible Raman scattering bands associated with the electrolyte were observed, as well as a slight increase in background fluorescence, due to the abundance of electrolyte in the Raman sampled volume in these regions. For this reason, we chose to perform *operando* experiments at these deeper focal positions (see Figure S3 for representative spectra at different spatial positions).

A typical Raman spectrum of the cell at open-circuit voltage (OCV) is shown in Figure 1d. Peaks are assigned based on literature data and by comparing the APC/THF spectrum with that of pure THF (see Figure S4). The peaks belonging to THF are the high-intensity peak at ~912 cm^{-1} (C_α−C_β asymmetric stretching) and a lower-intensity peak at ~1028 cm^{-1} (C_α−C_β symmetric stretching). A peak at ~210 cm^{-1} is also observed, which is associated with solvated Mg−Cl cationic species present in the electrolyte.[23] The peak at ~996 cm^{-1} arises from the ring-breathing mode of the phenyl groups in the $[AlPh_4]^-$ anion.[19,24]

Following measurements at OCV, Raman spectra were collected at a single position on the Pt gauze (lower surface, as discussed above) while the cell was subjected to potentiodynamic cycling between 2.2 V and −0.75 V. Each spectrum effectively represents the response averaged over a potential interval of 200 mV (see Methods in the Supporting Information for details on *operando* cycling procedure). Individual Raman spectra as a function of cell voltage are shown in Figure 2a after background subtraction and with intensity normalized to the most intense peak at ~912 cm^{-1} (this solvent peak was found to undergo minimal absolute intensity changes during cycling). Qualitative assessment of this plot indicates that the anion band at 996 cm^{-1} undergoes a decrease in relative intensity as the potential of the Pt gauze enters the plating region, and this is reversed with stripping. Less pronounced changes are also observed for the THF C_α−C_β symmetric stretching band at 1028 cm^{-1}. Close inspection of the low-frequency region of the spectrum also reveals some subtle changes in the Mg−Cl peak intensity at ~210 cm^{-1} during Mg plating potentials, as well as some other very weak intensity spectral features emerging in the 250−400 cm^{-1} region, but the weak signal:noise ratio makes any confident interpretation challenging (see Figure S5).

To understand the spectral evolution further, we present the cell voltage and current profile during the first four cycles of the *operando* experiment (Figure 2b,c) along with key Raman metrics derived from fitting the spectra (Figures 2d,e and S6a) as a function of time. The relative intensity (vs the THF mode at 912 cm^{-1}) of the $[AlPh_4]^-$ peak at 996 cm^{-1} clearly tracks the current (Figure 2d), with a decrease in intensity observed during Mg plating, followed by an increase during Mg stripping, before returning to its initial value. This behavior is observed across multiple cycles, with a slight increase in relative intensity with cycle number reflecting the increasing current with successive cycling. Plotting this relative intensity

https://doi.org/10.1021/acsenergylett.3c00279
ACS Energy Lett. XXXX, XXX, XXX−XXX

against the current (Figure S6b) shows a pair of hysteresis loops centered at zero current, whereby the Raman intensity lags the current response in both the positive and negative current directions (see discussion below). We also note that the peak at 1028 cm^{-1}, associated with the THF solvent, shows some evolution with cell voltage, but these are small in comparison to those observed for the $[AlPh_4]^-$ anion (see Figure S6a).

The intensity variations observed for the 996 cm^{-1} band can be interpreted as local concentration changes due to transport of the $[AlPh_4]^-$ anions away from/toward the Pt gauze electrode surface under the influence of migration during cycling. During Mg plating, the negative potential at the interface results in electrostatic repulsion of the anion from the Raman sampled region, while the opposite occurs during Mg stripping. The hysteresis can be explained by the time-lag between interfacial electron transfer and full development of the depletion layer in the volume of solution adjacent to the electrode surface that is sampled by the Raman measurement. While accurate quantification of this time lag is challenging, we estimate the offset observed between current and spectral response to be of the order of 200 s. The observed behavior is consistent with our previous *operando* ATR-FTIR measurements, adding further confidence to this interpretation, with the added benefit that the Raman experiments allow for spatial variations across the sample to be monitored on the microscale.

In addition to the isolated changes in the $[AlPh_4]^-$ band at 996 cm^{-1} with cell cycling, we also observe substantial variations in the background intensity, with a broad curved baseline feature exhibiting a maximum at approximately 500 cm^{-1} appearing in the raw spectra (Figure S7). The background intensity evolves with cell voltage and reveals a periodic trend with cycling (Figure 2e). It exhibits a sharp increase during the first plating cycle and reaches a maximum at the negative potential vertex (−0.75 V) before decreasing toward a plateau. The intensity then begins to fall back to the initial value but only once the stripping process is complete and no current is flowing in the cell. Similar changes are observed on subsequent cycles, albeit with a successive decrease in magnitude. Importantly, the background intensity returns to the initial value after each cycle, indicating that the responsible process is reversible.

Spectral backgrounds are common in Raman spectroscopy and are typically ascribed to fluorescence. We intentionally selected 830 nm as the excitation laser in order to minimize the intrinsic fluorescent background associated with the APC electrolyte under OCV conditions, but this background was found to vary under *operando* conditions. This may be due to chemical changes in the electrolyte or formation of a solid electrolyte interface (SEI) at the Pt electrode surface.[25,26] An alternative explanation is electronic Raman scattering (ERS), wherein photons are inelastically scattered by the conduction electrons in a metallic surface, resulting in a background continuum signal.[27,28] This phenomenon has been discussed more widely in the context of surface enhanced Raman scattering (SERS) at plasmonically active metals.[29] However, here we consider the possibility that Mg deposition on the Pt electrode results in an ERS background signal that varies periodically with cycling. A strong indicator for this association with Mg deposition is the fact that the background returns to its original intensity only after the Mg stripping phase is complete.

To explore the background variation further, we measured the Raman spectrum of pure, freshly polished Mg metal (see Figure S8), and at an excitation wavelength of 830 nm, we observe a broad and intense band centered at approximately 650 cm^{-1}. This is similar to the background response observed in our *operando* data (Figure S9), with a shift in peak position which possibly arises due to differences in surface morphology. The strong intensity of the background scattering signal observed on Mg metal suggests that the background variations observed in our *operando* measurements can be attributed to the varying coverages of deposited Mg present on the Pt surface throughout the potentiodynamic scan. Furthermore, a band is observed on Mg metal at 120 cm^{-1} (Figure S8a−c), and the tail of a band is also observed in this spectral region under Mg plating conditions during the *operando* experiment (Figure S5), although we were unable to make a confident assignment of this band. We also performed control measurements on $MgCl_2$, which do not exhibit any broad background signals at 830 nm excitation, confirming that the background phenomena that we observed is associated specifically with Mg in its metallic form. It is unclear whether this background effect arises purely through the ERS mechanism or includes some contribution from fluorescence. However, the reversibility of the background intensity profile combined with the known stability of the APC electrolyte under these conditions[13,14] suggests that fluorescence from electrolyte degradation or SEI formation is less likely than the ERS mechanism to be the primary origin of the background variations. Irrespective of the mechanism, our evidence suggests that the background intensity may offer a means to probe the Mg plating−stripping process at the electrode/electrolyte interface, but further investigation is required to understand the sensitivity of the background intensity to Mg coverage and surface morphology.

Our observations suggest that the *operando* Raman measurements are able to simultaneously provide dynamic information on both the anion transport in the electrolyte (using the $[AlPh_4]^-$ band at 996 cm^{-1}) and the Mg plating and stripping dynamics at the working electrode surface (using the background intensity at 500 cm^{-1}). This is also supported by time-series OCV relaxation experiments on a Pt gauze electrode after Mg plating (Figure S10), which showed relatively rapid (∼200 s) recovery of the $[AlPh_4]^-$ band intensity, in contrast to a drop in background scattering intensity at 500 cm^{-1} observed over much longer time scales (10^5 s), presumably indicating some instability to the Mg-plated Pt interface. To establish how independently the transport and plating−stripping phenomena can be probed, and to explore the repeatability of our experiments, we performed further *operando* measurements at different spatial locations on the Pt gauze working electrode (see Figure S3). Over five separate experiments we found that the cyclic changes in the $[AlPh_4]^-$ band intensity at 996 cm^{-1} were minimal (<10%) in three cases, while in the remaining two experiments the magnitude of the $[AlPh_4]^-$ band intensity change varied between 30% and 60% of the initial value. Conversely, the background intensity changes were clearly evident in all experiments, albeit with differences in magnitude (ranging between 25% and 80% change in initial intensity) and profile shape.

An example of this is shown in Figure S11, in which none of the electrolyte bands (including the $[AlPh_4]^-$ band at 996 cm^{-1}) exhibit periodic intensity changes with cycling, while the background intensity at 500 cm^{-1} exhibits a cyclic profile

https://doi.org/10.1021/acsenergylett.3c00279
ACS Energy Lett. XXXX, XXX, XXX−XXX

similar to Figure 2e. The absence of a statistical correlation between the $[AlPh_4]^-$ band intensity at 996 cm^{-1} and the background intensity supports our hypothesis that these two metrics are independently interrogating different aspects of the electrochemical process. We hypothesize that the reason for the large variations in the $[AlPh_4]^-$ electrolyte bands across different *operando* experiments is caused by the sensitivity of the measurement to the local mass transport regime at the electrode surface. The rates of electrolyte depletion and diffusional replenishment will intimately depend on the specific geometry surrounding the volume sampled in the Raman measurement. The spatial complexity of the Pt gauze working electrode and its proximity to the window of the spectroelectrochemical cell will affect these rates in a spatially dependent manner, leading to substantial heterogeneity in the *operando* Raman response. Conversely, Mg plating and stripping is common to all areas of the Pt electrode, and hence, the background variations are ubiquitous across all measurements.

We thus demonstrate that *operando* Raman spectroscopy can be used to independently investigate both interfacial processes and mass transport effects by separating the broad background scattering associated with Mg plating and stripping from spectroscopic Raman signature variations attributed to electrolyte ion migration. This is a significant finding because Raman background signals are typically disregarded or intentionally minimized through appropriate choice of excitation wavelength or more advanced instrumentation.[30,31] However, we see here that there may be valuable information embedded within the background response, and we envisage that this method could be applicable to other electrolyte systems containing suitable Raman active modes. Further work is ongoing to understand the mechanistic origin of the background signals and to establish their sensitivity to the morphology and thickness of Mg deposits.

■ ASSOCIATED CONTENT

Supporting Information

The Supporting Information is available free of charge at https://pubs.acs.org/doi/10.1021/acsenergylett.3c00279.

Materials and methods; spectroelectrochemical cell and cyclic voltammetry using the spectroelectrochemical cell for multiple cycles; experimental details of Raman spectroscopy measurement, *operando* experiment setup, and fitting models used; fitting parameters derived from two different fitting models employed; comparison of spectral metrics derived from two different fitting models and their evolution with cycling; spatial variation in spectral data across the working electrode interface; Raman spectrum of pure THF; low wavenumber region of *operando* Raman spectra, before and after baseline correction; variation of absolute peak intensities during electrochemical cycling and variation of peak ratios with measured current; variation of background intensity during electrochemical cycling; spectra of Mg metal and $MgCl_2$ under different laser excitations; comparison between Raman spectrum of pure Mg, Mg in THF, and *operando* spectrum obtained in the plating region; relaxation experiments showing recovery of potential from fully stripped conditions and associated changes in Raman spectra; *operando* data from a separate set of experiments showing baseline variation but no change in electrolyte peak ratios (PDF)

■ AUTHOR INFORMATION

Corresponding Author

Andrew J. Wain − *National Physical Laboratory, Teddington TW11 0LW, United Kingdom;* orcid.org/0000-0002-8666-6158; Email: andy.wain@npl.co.uk

Authors

Rudra N. Samajdar − *National Physical Laboratory, Teddington TW11 0LW, United Kingdom; WestCHEM, Department of Pure & Applied Chemistry, University of Strathclyde, Glasgow G1 1XL, United Kingdom;* orcid.org/0000-0002-5737-4906

Sofia Marchesini − *National Physical Laboratory, Teddington TW11 0LW, United Kingdom;* orcid.org/0000-0002-5051-0936

Scott A. Brown − *National Physical Laboratory, Teddington TW11 0LW, United Kingdom; WestCHEM, Department of Pure & Applied Chemistry, University of Strathclyde, Glasgow G1 1XL, United Kingdom*

Stuart D. Robertson − *WestCHEM, Department of Pure & Applied Chemistry, University of Strathclyde, Glasgow G1 1XL, United Kingdom;* orcid.org/0000-0002-9330-8770

Keith R. Paton − *National Physical Laboratory, Teddington TW11 0LW, United Kingdom;* orcid.org/0000-0003-0300-8676

Andrew J. Pollard − *National Physical Laboratory, Teddington TW11 0LW, United Kingdom;* orcid.org/0000-0002-6841-2592

Complete contact information is available at: https://pubs.acs.org/10.1021/acsenergylett.3c00279

Author Contributions

‡R.N.S. and S.M. contributed equally.

Notes

The authors declare no competing financial interest.

■ ACKNOWLEDGMENTS

This work was funded by the National Measurement System of the UK Department of Business, Energy and Industrial Strategy and the EPSRC Impact Accelerator Account (grant code EP/R51178X/1). The authors thank Dr. Alexander H. Shard for critical comments on the manuscript and Dr. Dimitrios Tsikritsis for help in setting up the *operando* experiments and useful comments on the Raman data.

■ REFERENCES

(1) Davis, S. J.; Lewis, N. S.; Shaner, M.; Aggarwal, S.; Arent, D.; Azevedo, I. L.; Benson, S. M.; Bradley, T.; Brouwer, J.; Chiang, Y.-M.; et al. Net-zero emissions energy systems. *Science* **2018**, *360*, eaas9793.

(2) Wang, F.; Harindintwali, J. D.; Yuan, Z.; Wang, M.; Wang, F.; Li, S.; Yin, Z.; Huang, L.; Fu, Y.; Li, L.; et al. Technologies and perspectives for achieving carbon neutrality. *Innovation* **2021**, *2*, 100180.

(3) Choi, J. W.; Aurbach, D. Promise and reality of post-lithium-ion batteries with high energy densities. *Nat. Rev. Mater.* **2016**, *1*, 16013.

(4) Winter, M.; Barnett, B.; Xu, K. Before Li ion batteries. *Chem. Rev.* **2018**, *118*, 11433−11456.

(5) Bucur, C. B.; Gregory, T.; Oliver, A. G.; Muldoon, J. Confession of a magnesium battery. *J. Phys. Chem. Lett.* **2015**, *6*, 3578−3591.

(6) Yoo, H. D.; Shterenberg, I.; Gofer, Y.; Gershinsky, G.; Pour, N.; Aurbach, D. Mg rechargeable batteries: an on-going challenge. *Energy Environ. Sci.* **2013**, *6*, 2265−2279.

(7) Song, J.; Sahadeo, E.; Noked, M.; Lee, S. B. Mapping the challenges of magnesium battery. *J. Phys. Chem. Lett.* **2016**, *7*, 1736−1749.
(8) Dominko, R.; Bitenc, J.; Berthelot, R.; Gauthier, M.; Pagot, G.; Di Noto, V. Magnesium batteries: Current picture and missing pieces of the puzzle. *J. Power Sources* **2020**, *478*, 229027.
(9) Liang, Z.; Ban, C. Strategies to enable reversible magnesium electrochemistry: from electrolytes to artificial solid−electrolyte interphases. *Angew. Chem., Int. Ed.* **2021**, *60*, 11036−11047.
(10) Xu, K. Electrolytes and interphases in Li-ion batteries and beyond. *Chem. Rev.* **2014**, *114*, 11503−11618.
(11) Gauthier, M.; Carney, T. J.; Grimaud, A.; Giordano, L.; Pour, N.; Chang, H.-H.; Fenning, D. P.; Lux, S. F.; Paschos, O.; Bauer, C.; et al. Electrode−electrolyte interface in Li-ion batteries: current understanding and new insights. *J. Phys. Chem. Lett.* **2015**, *6*, 4653−4672.
(12) Grey, C. P.; Tarascon, J. M. Sustainability and in situ monitoring in battery development. *Nat. Mater.* **2017**, *16*, 45−56.
(13) Samajdar, R. N.; Brown, S. A.; Kairy, S. K.; Robertson, S. D.; Wain, A. J. Methodologies for Operando ATR-IR Spectroscopy of Magnesium Battery Electrolytes. *Anal. Chem.* **2022**, *94*, 14985−14993.
(14) Brown, S. A.; Cussen, S. A.; Kennard, R.; Marchesini, S.; Pryke, J. J.; Rae, A.; Robertson, S. D.; Samajdar, R. N.; Wain, A. J. Atom-efficient synthesis of a benchmark electrolyte for magnesium battery applications. *Chem. Commun.* **2022**, *58*, 12070−12073.
(15) Rosser, T. E.; Dickinson, E. J. F.; Raccichini, R.; Hunter, K.; Searle, A. D.; Kavanagh, C. M.; Curran, P. J.; Hinds, G.; Park, J.; Wain, A. J. Improved Operando Raman Cell Configuration for Commercially-Sourced Electrodes in Alkali-Ion Batteries. *J. Electrochem. Soc.* **2021**, *168*, 070541.
(16) Weiling, M.; Pfeiffer, F.; Baghernejad, M. Vibrational Spectroscopy Insight into the Electrode| electrolyte Interface/Interphase in Lithium Batteries. *Adv. Energy Mater.* **2022**, *12*, 2202504.
(17) Wang, Y.-H.; Zheng, S.; Yang, W.-M.; Zhou, R.-Y.; He, Q.-F.; Radjenovic, P.; Dong, J.-C.; Li, S.; Zheng, J.; Yang, Z.-L.; et al. In situ Raman spectroscopy reveals the structure and dissociation of interfacial water. *Nature* **2021**, *600*, 81−85.
(18) Wang, Y.; Chen, D. Application of Advanced Vibrational Spectroscopy in Revealing Critical Chemical Processes and Phenomena of Electrochemical Energy Storage and Conversion. *ACS Appl. Mater. Interfaces* **2022**, *14*, 23033−23055.
(19) Pour, N.; Gofer, Y.; Major, D. T.; Aurbach, D. Structural analysis of electrolyte solutions for rechargeable Mg batteries by stereoscopic means and DFT calculations. *J. Am. Chem. Soc.* **2011**, *133*, 6270−6278.
(20) Vestfried, Y.; Chusid, O.; Goffer, Y.; Aped, P.; Aurbach, D. Structural analysis of electrolyte solutions comprising magnesium−aluminate chloro− organic complexes by Raman spectroscopy. *Organometallics* **2007**, *26*, 3130−3137.
(21) Salama, M.; Shterenberg, I.; J.W. Shimon, L.; Keinan-Adamsky, K.; Afri, M.; Gofer, Y.; Aurbach, D. Structural analysis of magnesium chloride complexes in dimethoxyethane solutions in the context of Mg batteries research. *J. Phys. Chem. C* **2017**, *121*, 24909−24918.
(22) See, K. A.; Liu, Y.-M.; Ha, Y.; Barile, C. J.; Gewirth, A. A. Effect of concentration on the electrochemistry and speciation of the magnesium aluminum chloride complex electrolyte solution. *ACS Appl. Mater. Interfaces* **2017**, *9*, 35729−35739.
(23) Liu, T.; Cox, J. T.; Hu, D.; Deng, X.; Hu, J.; Hu, M. Y.; Xiao, J.; Shao, Y.; Tang, K.; Liu, J. A fundamental study on the $[(\mu\text{-Cl})_3\text{Mg}_2(\text{THF})_6]^+$ dimer electrolytes for rechargeable Mg batteries. *Chem. Commun.* **2015**, *51*, 2312−2315.
(24) Socrates, G. *Infrared and Raman characteristic group frequencies: tables and charts*; John Wiley & Sons, 2004.
(25) Weaving, J. S.; Lim, A.; Millichamp, J.; Neville, T. P.; Ledwoch, D.; Kendrick, E.; McMillan, P. F.; Shearing, P. R.; Howard, C. A.; Brett, D. J. L. Elucidating the sodiation mechanism in hard carbon by operando raman spectroscopy. *ACS Appl. Energy Mater.* **2020**, *3*, 7474−7484.
(26) Ren, X.; Wang, J.; Peng, Z.; Lu, L. Direct monitoring of trace water in Li-ion batteries using operando fluorescence spectroscopy. *Chem. Sci.* **2018**, *9*, 231−237.
(27) Inagaki, M.; Isogai, T.; Motobayashi, K.; Lin, K.-Q.; Ren, B.; Ikeda, K. Electronic and vibrational surface-enhanced Raman scattering: from atomically defined Au (111) and (100) to roughened Au. *Chem. Sci.* **2020**, *11*, 9807−9817.
(28) Kamimura, R.; Kondo, T.; Motobayashi, K.; Ikeda, K. Surface-Enhanced Electronic Raman Scattering at Various Metal Surfaces. *Phys. Status Solidi B* **2022**, *259*, 2100589.
(29) Hugall, J. T.; Baumberg, J. J. Demonstrating photoluminescence from Au is electronic inelastic light scattering of a plasmonic metal: the origin of SERS backgrounds. *Nano Lett.* **2015**, *15*, 2600−2604.
(30) Cabo-Fernandez, L.; Neale, A. R.; Braga, F.; Sazanovich, I. V.; Kostecki, R.; Hardwick, L. J. Kerr gated Raman spectroscopy of $LiPF_6$ salt and $LiPF_6$-based organic carbonate electrolyte for Li-ion batteries. *Phys. Chem. Chem. Phys.* **2019**, *21*, 23833−23842.
(31) Neale, A. R.; Milan, D. C.; Braga, F.; Sazanovich, I. V.; Hardwick, L. J. Lithium Insertion into Graphitic Carbon Observed via Operando Kerr-Gated Raman Spectroscopy Enables High State of Charge Diagnostics. *ACS Energy Lett.* **2022**, *7*, 2611−2618.

https://doi.org/10.1021/acsenergylett.3c00279
ACS Energy Lett. XXXX, XXX, XXX−XXX